Analysis of Video Disdrometer and Polarimetric Radar Data to Characterize Rain Microphysics in Oklahoma

QING CAO AND GUIFU ZHANG

School of Meteorology, University of Oklahoma, Norman, Oklohoma

EDWARD BRANDES

National Center for Atmospheric Research,* Boulder, Colorado

TERRY SCHUUR AND ALEXANDER RYZHKOV

Cooperative Institute for Mesoscale Meteorological Studies, Norman, Oklahoma

KYOKO IKEDA

National Center for Atmospheric Research, Boulder, Colorado

(Manuscript received 7 March 2007, in final form 2 January 2008)

ABSTRACT

In this paper, data from three 2-dimensional video disdrometers (2DVDs) and an S-band polarimetric radar are used to characterize rain microphysics in Oklahoma. Sampling errors from the 2DVD measurements are quantified through side-by-side comparisons. In an attempt to minimize the sampling errors, a method of sorting and averaging based on two parameters (SATP) is proposed. The shape–slope (μ–Λ) relation of a constrained gamma (C-G) model is then refined for the retrieval of drop size distributions (DSDs) from polarimetric radar measurements. An adjustable term that is based on observed radar reflectivity and differential reflectivity is introduced to make the C-G DSD model more applicable. Radar retrievals using this improved DSD model are shown to provide good agreement with disdrometer observations and to give reasonable results, including in locations near the leading edge of convection where poorly sampled large drops are often observed.

1. Introduction

Rain microphysics can be characterized through joint disdrometer and polarimetric radar observations, where in situ measurements from the disdrometer provide information on individual drop sizes, shapes, and terminal velocities; also, remote measurements from radar provide information on the bulk precipitation characteristics over a wide area. In recent years, much progress has been made in developing drop size distribution (DSD) models, retrieving DSD parameters from polarimetric radar measurements, and quantitatively comparing the disdrometer measurements with the radar retrievals (e.g., Haddad et al. 1997; Bringi et al. 2002, 2003; Gorgucci et al. 2002; Brandes et al. 2004a,b; Vivekanandan et al. 2004; Zhang et al. 2001, 2006). In this study, we further demonstrate the potential of joint disdrometer–radar observations to improve quantitative precipitation estimation and microphysical parameterization.

DSDs are usually modeled by a gamma distribution (Ulbrich 1983) as

$$N(D) = N_0 D^\mu \exp(-\Lambda D), \tag{1}$$

where N_0 (mm$^{-1-\mu}$ m^{-3}) is a number concentration parameter, μ is a distribution shape parameter, Λ (mm^{-1}) is a slope parameter, and D (mm) is the equiva-

lent volume diameter. Several researchers (e.g., Ulbrich 1983; Chandrasekar and Bringi 1987; Haddad et al. 1997) have shown that the three parameters (N_0, μ, and Λ) of a gamma function fit are not mutually independent. Ulbrich (1983) introduced an N_0–μ relation whereby the three DSD parameters could be retrieved using radar measurements of radar reflectivity (Z_H) and attenuation. However, the N_0–μ relation, depending on the fitting procedure, is unstable and fluctuates by several orders of magnitude, and therefore its utility is limited. Chandrasekar and Bringi (1987) attributed the N_0–μ relation to statistical error. Haddad et al. (2006) further showed that even in the absence of observation noise, the dual-frequency retrieval using a N_0–μ relation could be ambiguous. Haddad et al. (1997) introduced a parameterization of gamma distribution, which has three mutually independent parameters. Realizing that there are 3 degrees of freedom for a gamma distribution, Bringi et al. (2002) proposed using polarimetric radar measurements of reflectivity, differential reflectivity (Z_{DR}), and specific differential phase (K_{DP}) to retrieve a normalized gamma DSD. However, Brandes et al. (2004b) showed that this approach is sensitive to K_{DP} noise. In addition, K_{DP} is derived from measurements made over many range gates and does not always match Z_H and Z_{DR} measurements well at every range gate. Therefore, the addition of K_{DP} may result in a deterioration of the DSD retrieval at a specific range gate, especially if it is not used optimally. Through disdrometer observations, Zhang et al. (2001) and Brandes et al. (2004a) found that μ is highly related to Λ. The resulting μ–Λ relationship can be used as a constraint that allows DSDs to be retrieved from dual-polarization or dual-frequency radar measurements. In general, this approach was proven to perform well for DSD retrieval (Vivekanandan et al. 2004; Brandes et al. 2004a,b; Zhang et al. 2006). Nevertheless, there are still several issues that need to be addressed, such as natural DSD variability, sampling errors, and the applicability of the DSD model.

The first issue examined in this paper is the quantification of disdrometer sampling errors related to small sampling volumes and limited sampling times. Disdrometer observations contain not only physical variation but also measurement errors. Gertzman and Atlas (1977) and Wong and Chidambaram (1985) presented a detailed analysis of sampling errors based on the assumption of independent Poisson distributions. Rain events, however, may not be independent stationary random processes. Physical variation and sampling errors coexist (e.g., Jameson and Kostinski 1998; Schuur et al. 2001). It is difficult to separate sampling errors from physical variations with a single instrument. Side-

by-side comparisons, on the other hand, provide information that allows sampling errors to be quantified. Tokay et al. (2001) compared measurements from a 2-dimensional video disdrometer (2DVD) and an impact disdrometer [the Joss–Waldvogel disdrometer (JWD)]. However, their study focused mainly on the comparison of DSD parameters and rain variables and did not quantify errors. To our knowledge, error quantification for 2DVD observations through side-by-side comparison has not yet been reported. By knowing observational errors and their error correlations for different DSD moments, the error propagation can be estimated for any rain variable estimator based on rain moments (e.g., Zhang et al. 2003). On the other hand, error quantification helps to introduce advanced processing techniques to reduce error effects on DSD modeling or retrieval.

It is well known that DSD variability can be reduced by averaging. For example, Joss and Gori (1978) demonstrated that random, time-sequential, and rain-rate sequential averaging will lead to exponential DSDs. Sauvageot and Lacaux (1995), considering "instantaneous" DSDs having strong variability, further studied averaged DSDs of JWD data within a set of rain-rate intervals and found that the rain rate–reflectivity (R–Z_H) relations obtained from averaged DSDs are close to those calculated from nonaveraged data and compatible with those proposed in previous studies. Lee and Zawadzki (2005) introduced the sequential intensity filtering technique (SIFT), which was to be used for processing a single rain event, by sorting DSDs within a time window (typically 1 h) by reflectivity and averaging consecutive DSDs (typically 10). They found that averaging DSDs within an interval of reflectivity could reduce observational errors of disdrometric measurements and yield more stable R–Z_H relations. The averaging methods mentioned above, however, apply a coarse filtering technique that results in a significant loss of physical variation. A better method to process disdrometer data is needed—one that can preserve physical variability while reducing the impact of observational error.

Although a DSD model can be readily developed based on disdrometer observations, the model may not always be applicable for retrieving DSDs from radar measurements. There are discrepancies between radar and disdrometer measurements that are attributable to factors such as rainfall inhomogeneity, sampling volume differences, limitations in radar measurements (e.g., contamination, sampling error, and miscalibration), limitations in disdrometer measurements (e.g., undersampling, splashing, and wind effects), and nonstationary rain processes (e.g., drop sorting, clustering,

and evaporation). If radar-measured reflectivity and differential reflectivity are close to calculations from disdrometer observations, radar retrievals based on a disdrometer-derived DSD model generally agree with in situ measurements. However, when radar measurements deviate greatly from disdrometer observations, especially for cases involving a relatively small reflectivity but large differential reflectivity, DSD retrievals by radar are not satisfactory. This demonstrates that, in some cases, an adjustment to the constrained gamma (C-G) DSD model is needed.

In this paper, we present data analyses and results of a joint disdrometer and polarimetric radar study. In section 2, disdrometer sampling errors are quantified by analyzing measurements from two instruments placed side-by-side. A sorting and averaging procedure based on two parameters (SATP) is introduced to mitigate the effects of sampling errors on DSD fitting. The C-G DSD model is then refined, and the microphysical properties of rains in Oklahoma are determined. In section 3, an adjustment of the disdrometer-derived μ–Λ relation is introduced. The refined DSD model is used to retrieve DSDs from polarimetric radar measurements. The validity of the refined μ–Λ relation is verified in sections 2 and 3. Conclusions are presented in section 4.

2. Disdrometer data analysis

Assuming that DSDs can be represented by the gamma distribution (1), rain microphysics can be characterized by finding the governing parameters of the distribution. The moment fit is widely used to retrieve DSD parameters (e.g., Kozu and Nakamura 1991; Ulbrich and Atlas 1998). In practice, because of the finite sample volume and sample time, only a finite number of raindrops are measured over a size interval (D_{min}, D_{max}). The nth moment of the DSD is calculated as

$$M_n = \int_{D_{min}}^{D_{max}} D^n N(D) \, dD. \quad (2)$$

This paper utilizes the second, fourth, and sixth moments to fit three gamma distribution parameters. This procedure uses the same equations that appear as Eqs. (3) and (6)–(8) in Vivekanandan et al. (2004) and is referred to as the truncated moment fit (TMF) in the following sections.

The disdrometer data analyzed in this study came from three 2DVDs operated by the University of Oklahoma (OU), the National Center for Atmospheric Research (NCAR), and the National Severe Storms Laboratory (NSSL), respectively. Radar data were collected with a polarimetric WSR-88D (KOUN) operated by

NSSL. All measurements were made in Oklahoma from May 2005 to May 2007. At times, the 2DVDs were placed at the Southern Great Plains site [Kessler Farm Field Laboratory, (KFFL)] of the Atmospheric Radiation Measurement Program, which is located approximately 28 km south of KOUN. This site was chosen for radar–disdrometer comparisons. Up to two 2DVDs were also deployed for periods at NSSL and near the town of Cement (about 76 km southwest of KOUN). The NCAR 2DVD was placed next to the NSSL 2DVD for a number of rain events (Brandes et al. 2005) and the OU 2DVD was also placed next to the NSSL 2DVD for one rain event. In all, 14 200 1-min drop spectra with drop counts greater than 50 were collected (March–May, 5297 min; June–August, 2681 min; September–November, 2753 min; December–February, 3469 min). The dataset also includes 435 min of side-by-side 2DVD measurements, which are used in this study to quantify sampling error.

a. Observed DSD and sampling errors

Disdrometer observations contain sampling errors that arise from a limited sampling volume. An example is shown in Fig. 1. Drop size distribution, mass distribution, and reflectivity distribution are shown in the subplots. A total of 525 drops were sampled. Although there were only four drops larger than 2.1 mm, those drops significantly contribute to the reflectivity. The measured DSD is fitted to the gamma distribution using the TMF method (solid line). Obviously, poor sampling of relatively large drops causes errors in high moment estimation and, subsequently, in the fitted DSD parameters. Poor sampling of large drops can clearly be a problem for 2DVDs, which have a sampling area of ~0.01 m^2 and a typical sampling volume of ~3 m^3 within 1 min.

In practice, it is difficult to separate sampling errors from physical variation for single disdrometer measurements. Measurements by two similar disdrometers deployed side-by-side, however, can be treated as two realizations x_1, x_2 of the same process having the same expected value. That is,

$$\begin{cases} x_1 = \langle x \rangle + \varepsilon_1 \\ x_2 = \langle x \rangle + \varepsilon_2, \end{cases} \quad (3)$$

where the notation "$\langle \, \rangle$" denotes the expected value and ε_1, ε_2 are errors. Assuming that two disdrometers measure the same DSD, any differences between two measurements would result from statistical fluctuations. The physical variation can be cancelled by subtracting one measurement from the other. Assuming that the sampling errors of the two disdrometers are independent, the sampling error can be quantified by
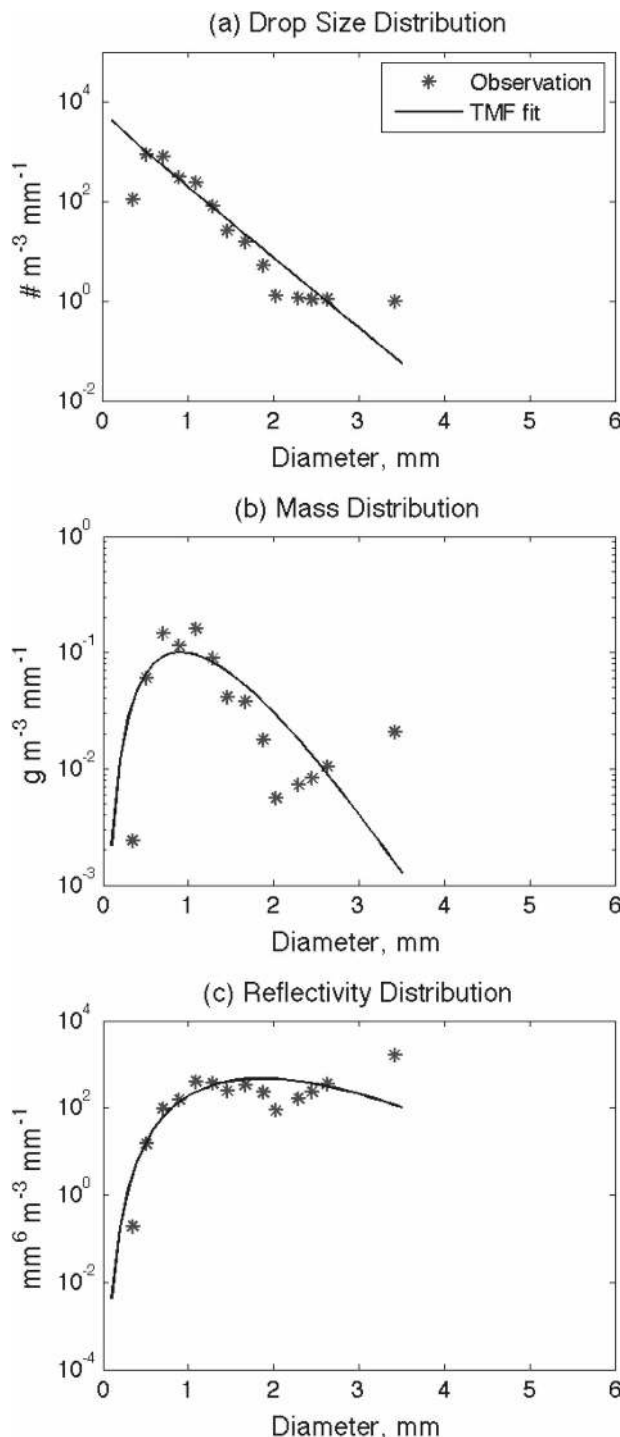
$$\langle |x_1 - x_2|^2 \rangle = \langle |\varepsilon_1 - \varepsilon_2|^2 \rangle = 2\sigma_x^2, \qquad (4)$$

where σ_x is the standard deviation of sampling errors. The error can also be represented by the fractional standard deviation (FSD) as

$$\mathrm{FSD}_x = \frac{\sigma_x}{\langle x \rangle}. \qquad (5)$$

The expected value of x is not known in practice. However, if the rain process is assumed to be a stationary random process, then the expected value of x could be estimated using the time-average of all available data based on ergodic theorem. In this paper, the expected value was estimated by taking the time-averaged value of 14 200 1-min samplings for Eqs. (4) and (5) and the formulas hereinafter. It is worthwhile to note that this kind of estimation introduces some uncertainties because in practice the rain process is not an ergodic process. Nevertheless, the uncertainty attributed to the time average is not the emphasis of this paper. Using this procedure, we processed the side-by-side 2DVD data to estimate the FSD.

Differences between two 2DVD measurements arise from spatial inhomogeneity in rain and slight differences in the spatial and temporal resolutions between the two units. Measurement bias is reduced by calibration. Measured number concentrations within each bin were averaged for both 2DVDs. For each bin, the difference between two mean number concentrations was regarded as a measurement bias. The measurement bias was then subtracted from the NSSL 2DVD measurements. Although the measurement bias cannot be perfectly tuned for bins with a size less than 0.6 mm, bias effects are insignificant for integral parameters. FSDs of physical parameters, such as drop count, mass, and reflectivity distributions, had similar error characteristics. Taking drop count measurements as an example, FSDs estimated using Eqs. (4) and (5) are denoted as "side-by-side" and are shown as a function of bin size (solid line) in Fig. 2. If only measurements of a single 2DVD are used, the standard deviation σ_x in Eq. (5) is calculated by $\sigma_x^2 = \langle |x - \langle x \rangle|^2 \rangle$. The dashed line represents the result of the NCAR 2DVD measurements, and the dashed–dotted line represents the result of the NSSL 2DVD measurements. The dashed and dashed–dotted lines agree well for the medium-sized drops. Based on the assumption that the observed raindrops obey the Poisson process, the theoretical FSDs, shown by the dotted–solid line, are derived by $\langle N_i \rangle^{-0.5}$, where N_i is the total number of drops within the ith bin.

As shown in Fig. 2, FSDs estimated from single 2DVD measurements (dashed and dashed–dotted lines) give an overestimation for sampling errors. Considering that side-by-side 2DVD measurements elimi-

FIG. 1. Example of a 1-min DSD with poor sampling (0922 UTC 13 May 2005). A total of 525 drops were sampled. The asterisks represent data points; the solid lines represent fitted distributions by TMF fit. (a) Drop size distribution; (b) mass distribution; (c) reflectivity distribution.
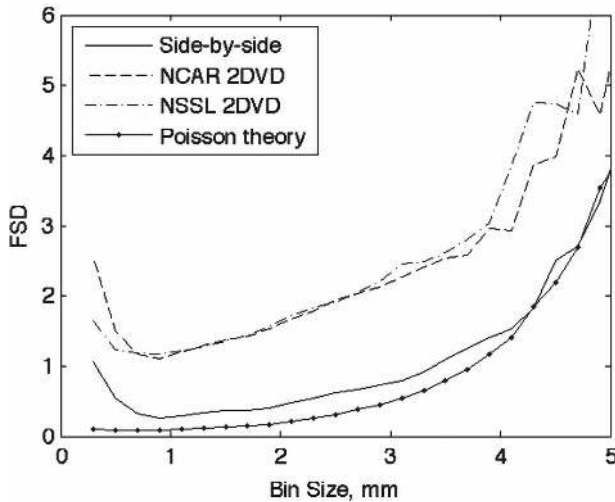
FIG. 2. FSD of observed drop counts over bin spectrum. The solid line represents the calculation based on side-by-side comparison; The dashed (dashed–dotted) line represents the result of NCAR (NSSL) 2DVD. The solid–dotted line represents the calculation based on Poisson assumption.

nate the physical variation, the sampling errors estimated this way are more accurate than from single 2DVD estimates. The difference between the solid and the dashed or dashed–dotted lines in Fig. 2 demonstrates the DSD's physical variability, which is large compared to the Poisson error (within bin sizes less than 3.5 mm). The solid line also shows that the sampling error increases with decreasing drop size for drops smaller than 0.6 mm. This is mainly attributed to the 2DVD's inability to accurately measure small drops. The dotted–solid line represents the Poisson error, which increases considerably when drop sizes are larger than 3 mm because of the undersampling of large raindrops. It is also noticed that the sampling error indicated by the solid line is close to the Poisson error for raindrop sizes greater than 3 mm. It implies that the sampling error is associated primarily with the undersampling for these sizes.

FSDs of DSD moments were estimated by applying Eqs. (4) and (5), in which the variable x represents the DSD moment (not bin drop counts). The results for moments from the 0th order to the 6th order are given in the columns of Table 1 ($M_0, M_1, \ldots, M_6$). The first row contains the result estimated from the side-by-side

comparison. The second row, labeled "Theoretical," contains the result estimated from the same dataset but based on the Poisson statistical model (Schuur et al. 2001, their appendix). Because the theoretical result assumes both that raindrop counts obey the Poisson distribution within a 1-min sampling interval and that the random process is independent, it gives a lower limit to the actual FSDs. The theoretical result indicates that moment errors are generally larger for higher moments. This can be explained by moment estimation; that is, because large drops carry more weight in the calculation of the higher moments, their sampling errors are greater contributors to the total error. The estimate from the side-by-side comparison generally agrees with this tendency except that the errors are a little larger. The difference between the side-by-side and theoretical results might be explained by (i) dependent measurement errors (i.e., samples from two adjacent times or bins have correlated errors), (ii) instrumental bias, and/or (iii) non-Poisson-distributed raindrops. Because error estimates in Table 1 were obtained directly from disdrometer measurements without any assumption regarding DSD shape, they are more realistic than results of simulations.

Correlations exist not only between DSD moments (e.g., Jameson and Kostinski 1998) but also between sampling errors of DSD moments (e.g., Zhang et al. 2003). Because the sampling errors have been quantified by a side-by-side comparison in this paper, the correlation between sampling errors can be quantified as well. The correlation coefficient is formulated by

$$\rho = \frac{\langle \varepsilon_m \varepsilon_n \rangle}{\sqrt{\langle \varepsilon_m^2 \rangle \langle \varepsilon_n^2 \rangle}}, \qquad (6)$$

where m and n represent two moments ($m, n = 0, \ldots, 6$) and ε denotes the error of observed moments. In practice, the $\langle \varepsilon_m \varepsilon_n \rangle$ is estimated from two 2DVDs measurements by $(1/N)\sum_{k=1}^{N} 0.5[x_{1,k}^{(m)} - x_{2,k}^{(m)}][x_{1,k}^{(n)} - x_{2,k}^{(n)}]$, where x denotes the measured moment, subscript 1, 2 represents two 2DVDs, and N is the number of side-by-side samples. Correlation coefficients between sampling errors for DSD moments ranging from the 0th to the 6th order are given in Table 2. It is obvious that sampling errors are less correlated if two moments are widely spaced. The correlation will be less than 10% if

TABLE 1. FSD of different rain moments.

Moment	M_0	M_1	M_2	M_3	M_4	M_5	M_6
Side-by-side	0.1029	0.0965	0.0906	0.0901	0.1025	0.1311	0.1746
Theoretical	0.0379	0.0350	0.0408	0.0550	0.0767	0.1045	0.1372

TABLE 2. Correlation coefficient of sampling errors for different moments.

	M_0	M_1	M_2	M_3	M_4	M_5	M_6
M_0	1	0.8927	0.6805	0.4996	0.3385	0.1927	0.0531
M_1	0.8927	1	0.9142	0.7202	0.5116	0.3449	0.2058
M_2	0.6805	0.9142	1	0.9160	0.7371	0.5594	0.3988
M_3	0.4996	0.7202	0.9160	1	0.9346	0.7927	0.6215
M_4	0.3385	0.5116	0.7371	0.9346	1	0.9493	0.8244
M_5	0.1927	0.3449	0.5594	0.7927	0.9493	1	0.9570
M_6	0.0531	0.2058	0.3988	0.6215	0.8244	0.9570	1

the order difference is larger than 6. Given the same order difference (e.g., correlation of M_0 and M_3 versus correlation of M_3 and M_6), the correlation tends to be a little larger for higher moments, which is caused by sampling errors. As for the second, fourth, and sixth moments, which were chosen to retrieve DSD parameters, the correlation coefficients for pairs M_2–M_4, M_4–M_6, and M_2–M_6 are 0.74, 0.82, and 0.40, respectively. It is important to know these FSDs and correlation coefficients because they determine the standard errors of DSD parameter estimates (Zhang et al. 2003).

b. DSD sorting and averaging based on two parameters

As shown in the previous subsection, sampling error is an unavoidable problem for 2DVD measurements, resulting in the degradation of the DSD fitting (Zhang et al. 2003). Because the DSD models are based on 2DVD observations (e.g., the C-G DSD model depends on fitted shape and slope parameters), the challenge is to reduce the sampling errors so that fitted shape and slope parameters are less affected by errors. Here, we suggest a sorting and averaging method based on two parameters. The SATP method is proposed because numerous 2DVD measurements are available with which to develop the constraining shape–slope relation of the C-G DSD model. Unlike the SIFT method introduced by Lee and Zawadzki (2005), SATP is applied to a whole dataset rather than a single event. With SATP, two parameters are used to characterize the DSD, and physical variability is therefore preserved much better than with SIFT. The SATP procedure is briefly described as follows:

 (i) Select two characteristic parameters to build two-dimensional grids,
 (ii) Calculate both characteristic parameters based on 1-min DSD measurements,
(iii) Sort the whole dataset and find DSDs with similar physical characteristics according to their two characteristic parameters,
(iv) Average the observed DSDs located in the same grid to obtain a new DSD, and

 (v) Process the averaged DSDs (i.e., fit them to a gamma distribution) to develop the shape–slope relation of the C-G DSD model.

The characteristic parameters can be any two rain variables (e.g., DSD moments, characteristic sizes of DSD, etc.). In general, the high moments, which have relatively larger measurement errors, and the low moments, which are determined by small drops and susceptible to disdrometer measurement uncertainty, do not represent rain physics well. On the other hand, the middle moments are both more representative of rain physics and more accurately measured. In this study, the middle moment–related parameters, rain rate (R) and median volume diameter (D_0), are therefore chosen for processing.

The sorting grids used in this study are shown in Fig. 3. Each grid in the R–D_0 plane is defined by variations of $\pm 5\%$ for R and ± 0.025 mm for D_0. The bar length indicates the number of observed DSDs. DSDs within each grid pixel are characterized by small variations of R and D_0 and are assumed to represent similar rain physics. For example, Fig. 4 shows three groups of observed DSDs (thin solid lines) within three different grids. The dashed, bold solid, and dashed–dotted lines represent three mean DSDs. For the three groups of DSDs in Fig. 4, FSDs of R are 5.58%, 11.82%, and 5.1%, FSDs of D_0 are 1.53%, 1.86%, and 0.76%, FSDs of total number concentration (N_T) are 1.75, 1.73, and 1.46 dB, and FSDs of Z_H are 1.57, 1.85, and 0.72 dB, respectively. These FSDs imply that SATP has the potential to identify similar DSDs. If we assume that the sorted DSDs within each grid pixel have the same DSD (expected value) and similar sampling error, the latter can surely be reduced by averaging the sorted DSDs. The fit to the averaged DSD is therefore less affected by errors and represents the physics better than the fit to nonaveraged DSDs. Compared to one-parameter filtering methods, SATP better preserves the physical variation.

A comparison of SATP with SIFT is shown in Fig. 5. The rain data were recorded by the OU 2DVD on 11 March 2007. The values of Z_H, R, D_0, and N_T, calcu-
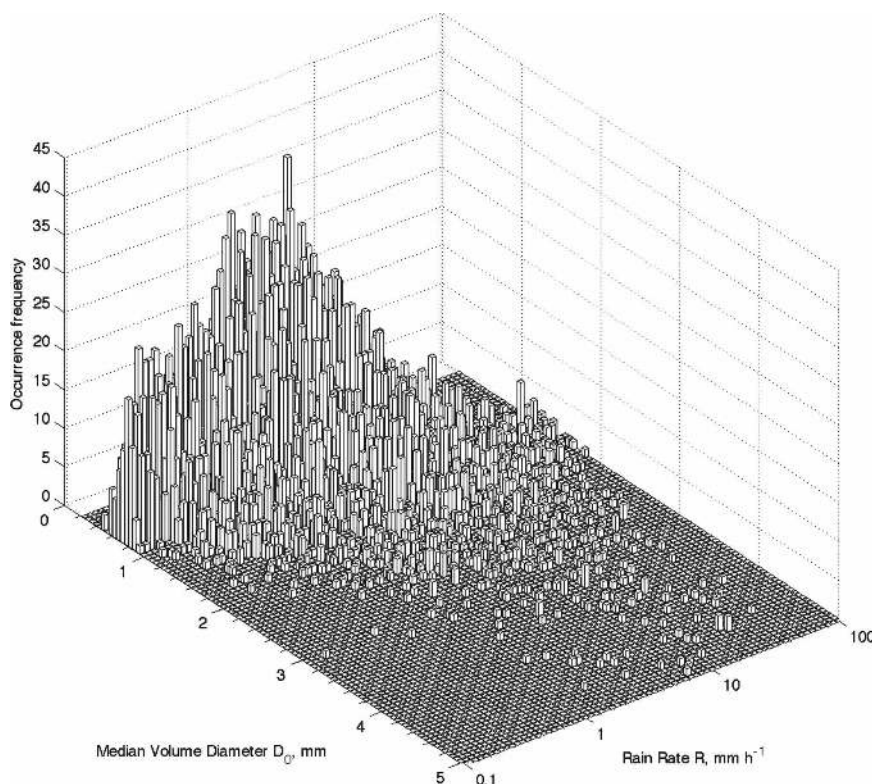
FIG. 3. Occurrence frequency of sorted rain data based on rain rate (step 10%) and median volume diameter (step 0.05 mm). Each pixel of the R–D_0 plane represents a specific DSD. The bar over the pixel denotes the number of observed DSDs sorted for one specific DSD. Observed DSDs within a pixel are averaged to obtain the specific DSD.
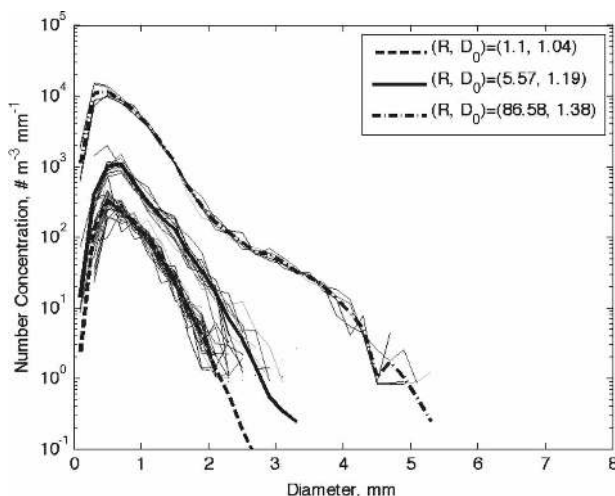

FIG. 4. Example of sorted DSDs and their mean DSDs. Thin solid lines represent the observed DSDs, which are sorted into three grids using SATP method. DSDs within one grid have a similar distribution. Three mean DSDs are denoted with the thick dashed, thick solid, and thick dashed–dotted lines; they represent rains with (R, D_0) = (1.1 mm h^{-1}, 1.04 mm), (5.57 mm h^{-1}, 1.19 mm), and (86.58 mm h^{-1}, 1.38 mm), respectively.

lated from observed DSDs, are plotted as dots in Fig. 5. The solid lines represent SATP results. For every 1-min observation, SATP processes the entire dataset to identify DSDs that are similar to the observed DSD and averages them to create a substitute for the observation. This averaged DSD is believed to reduce sampling errors because SATP combines useful information from other similar DSDs. The dashed lines represent variables calculated by SIFT, which sorts Z_H (within a time period of 4.5 h) by an increasing sequence and averages 10 adjacent DSDs to obtain the mean DSD. As shown in Fig. 5, the SATP results match observations well for all rain variables and maintain the physical variations, whereas for SIFT only Z_H (a high moment) preserves the observational variability. Other variables, especially the zero moment N_T, deviate considerably from observations.

SATP is a strategy for processing large amounts of raw data that contain errors. Because it is hard to exactly quantify the error reduction of each individual grid, we do not intend to use SATP to analyze "instantaneous" integral rain parameters as shown in Fig. 5.
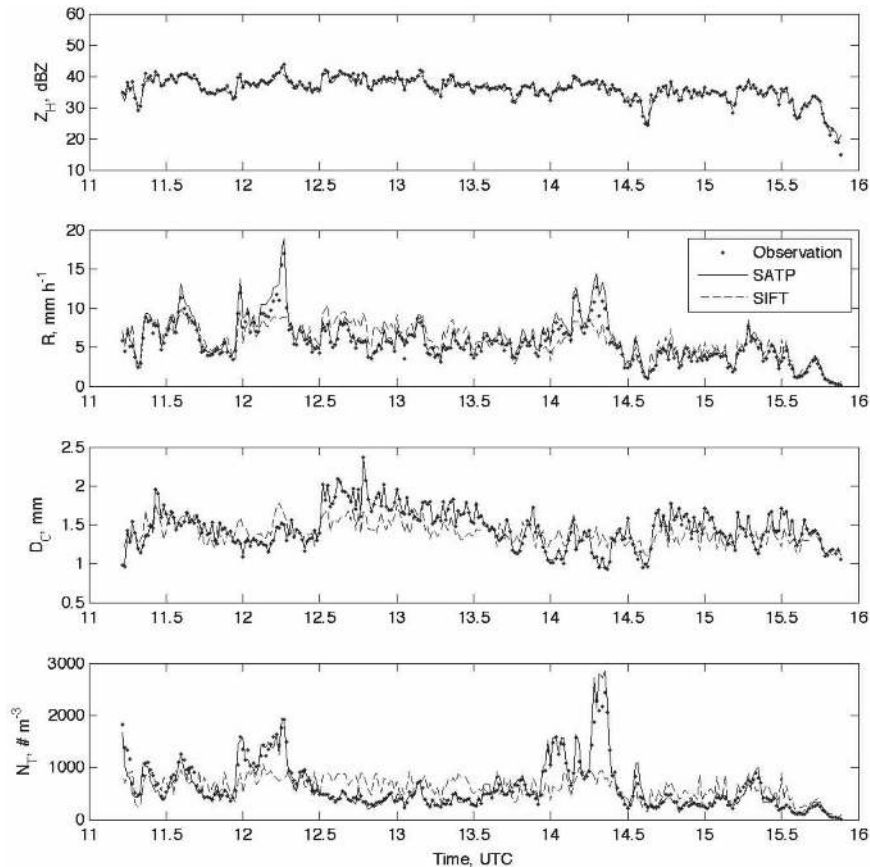
FIG. 5. Comparison of SATP and SIFT methods on reflectivity Z_H, rain rate R, median volume diameter D_0, and total number concentration N_T. Dots denote the data point observed at KFFL by OU 2DVD on 11 Mar 2007. Solid (dashed) lines denote calculations using the SATP (SIFT) method.

SATP is designed to provide the mean property of the DSD (i.e., the mean μ–Λ relation) rather than to improve on the individual observation. Because the physics is preserved with less error, the mean μ–Λ relation processed by SATP is obviously better than that obtained directly from error-contaminated measurements. Determining the error reduction for a specific DSD is not the major concern. On the other hand, the frequency distribution (Fig. 3) shows that rain data ($R < 3$ mm h^{-1}) account for a large portion of the dataset. The μ–Λ relation derived from the data prior to SATP filtering will be largely controlled by those data. Fitted DSDs of light rains always have large μ and Λ, and unfiltered results will raise the slope of the mean μ–Λ relation and cause the retrieval using the μ–Λ relation to deteriorate. SATP reduces the effects of light rain events and represents other rain events well. It is worthwhile to note that the SATP could be improved if more parameters (e.g., three parameters) were used to sort the similar DSDs. In this study, the dataset was not sufficient to do that, so only two parameters were ap-

plied. In the next section, we apply SATP to derive a constrained μ–Λ relation.

c. Refined shape–slope relation

The shape–slope relation of the C-G DSD model may vary in different climate regions. Our previous studies (e.g., Zhang et al. 2001; Brandes et al. 2004a,b) have shown that the relation for the southern Great Plains (i.e., Oklahoma) is a little different than the one for a subtropical region (i.e., Florida). Using the SATP method, 2DVD data were processed to refine the μ–Λ relation for rains in Oklahoma. First, the data were grouped on an R–D_0 grid and averaged. Averaged DSDs were then fitted to a gamma distribution by the TMF method. After that, the second-order polynomial least-square fit was used to obtain the mean μ–Λ relation. The fitted μ and Λ for the sorted and averaged DSDs are plotted in Fig. 6. The solid line is the fitted curve of circle points, and a dashed line depicts the Florida μ–Λ relation from Zhang et al. (2001). The dashed line generally has larger values for μ than the
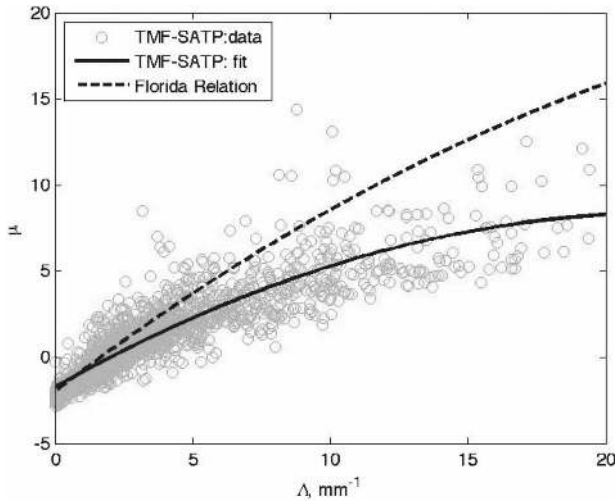
FIG. 6. Scatterplots of μ–Λ with DSD sorting. Circles denote DSD data fitted by TMF method. The solid line is the mean curve fitted to circle points by two-order polynomial fit; the dashed line corresponds to the Florida relation (Zhang et al. 2001).

solid line, given the same Λ, which implies that DSDs in Florida tend to have a narrower shape than DSDs in Oklahoma. The solid line in Fig. 6 is the refined μ–Λ relation of C-G DSD model used for DSD retrieval and is given by

$$\mu = -0.0201\Lambda^2 + 0.902\Lambda - 1.718. \qquad (7)$$

Equation (7) is applicable for a Λ within a range from 0 to 20. Larger Λ values are thought to result from measurement errors rather than storm physics (Zhang et al. 2003).

To verify the refined μ–Λ relation, we examine the mean mass-weighted diameter (D_m) and standard deviation of the mass-weighted diameter distribution (σ_m) because both can be directly derived from observations and are independent of sorting and fitting procedures. If relation (7) represents rain physics, the D_m–σ_m relation derived from observations and from relation (7) should be consistent. Figure 7a shows the result of these
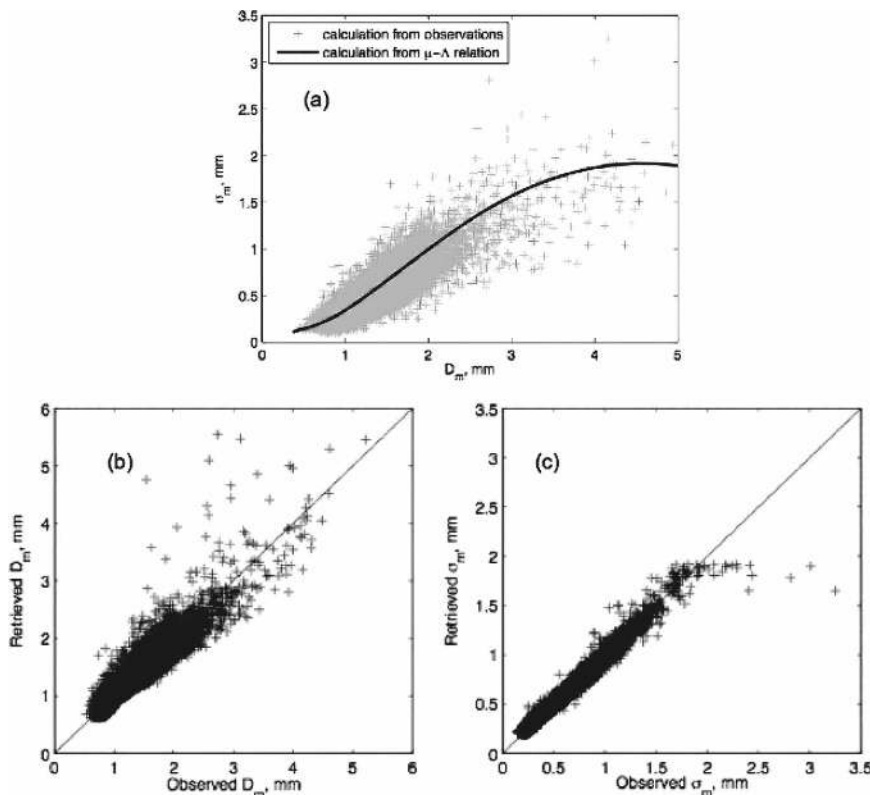

FIG. 7. (a) Scatterplots of D_m vs σ_m. Circles denote that D_m and σ_m are calculated from observed DSDs of 14 200 min. The solid line denotes that D_m and σ_m are calculated from gamma DSDs with μ–Λ constrained by Eq. (7). (b) One-to-one plot of retrieved D_m vs observed D_m using Eq. (7). Crosses denote the data points and the solid line corresponds to the unit slope. The bias is -2.18% and the correlation coefficient is 0.915. (c) As in (b) but for retrieved and observed σ_m. The bias is -1.15% and the correlation coefficient is 0.985.

TABLE 3. Bias and correlation coefficient for retrieved rain variables vs observations.

	D_m	σ_m	W	R	D_0	N_T
Bias (%)	−2.18	−1.15	2.52	3.37	8.73	14.16
Correlation coef	0.915	0.985	0.967	0.986	0.819	0.763

calculations. Crosses denote calculations of D_m and σ_m from observed 1-min DSDs. The solid line, derived from relation (7), agrees with observations.

Further verification was done by combining calculated Z_H and Z_{DR} and (7) and then retrieving D_m and σ_m. One-to-one plots of the retrieved and observed D_m and σ_m are shown in Figs. 7b,c. Some data points deviate substantially from the solid line (e.g., observed σ_m larger than 2.4 mm). These data points typically are DSDs with long and poorly sampled tails (not shown). However, the outliers are few in number and do not contaminate the result. The bias between retrieval values and observed values is calculated by $\langle y \rangle - \langle x \rangle$, where x is the observation and y is the retrieval value. The correlation coefficient is calculated by $\text{Cov}(x, y)/\sqrt{\text{Cov}(x, x) \times \text{Cov}(y, y)}$, where Cov is the covariance. The bias of retrieved D_m using relation (7) is only −0.03 mm (or −2.18%) and the correlation coefficient is 0.915 (Fig. 7b), whereas the bias of retrieved σ_m is only −0.007 mm (or −1.15%) and the correlation coefficient is 0.985 (Fig. 7c). The same comparison procedure can be applied for rain variables of liquid water content (W), R, D_0, and N_T. For observations with $R <$ 100 mm h^{-1}, Table 3 lists bias and correlation values of retrievals versus observations for several rain variables. Except for N_T, all these variables have a small bias and a correlation coefficient close to 1. These results show that the refined μ–Λ relation in Eq. (7) is valid for the rain DSD retrieval.

d. Parameterization of rain microphysics

Using the constraining μ–Λ relation in Eq. (7), relations between rain variables and radar variables can be derived following the procedure described by Brandes et al. (2004b) and Zhang et al. (2006). Errors, however, may propagate through this procedure. Fitting directly with observations (without using the constraining μ–Λ relation) should reduce error propagation. Based on DSD data processed with the SATP method, rain variables [liquid water content (g m^{-3}), rainfall rate (mm h^{-1}), total number concentration (m^{-3}), and median volume diameter (mm)] were calculated for each data point. Radar reflectivity (in linear units of mm^6 m^{-3}) and differential reflectivity (dB) were calculated as well. Using a polynomial fit for all data points, rain

variables were expressed in terms of radar variables as (see also Figs. 8a–c)

$$N_T = Z_H \times 10^{(-0.0837Z_{DR}^3 + 0.702Z_{DR}^2 - 2.062Z_{DR} + 0.794)}, \tag{8}$$

$$R = Z_H \times 10^{(-0.0363Z_{DR}^3 + 0.316Z_{DR}^2 - 1.178Z_{DR} - 1.964)}, \tag{9}$$

$$W = Z_H \times 10^{(-0.0493Z_{DR}^3 + 0.430Z_{DR}^2 - 1.524Z_{DR} - 3.019)} \quad \text{and} \tag{10}$$

$$D_0 = 0.0436Z_{DR}^3 - 0.216Z_{DR}^2 + 1.076Z_{DR} + 0.659. \tag{11}$$

Rain microphysical processes can be estimated if the DSD is known. Following the procedure described by Zhang et al. (2006), the evaporation rate (R_e, g m^{-3} s^{-1}), accretion rate (R_a, g m^{-3} s^{-1}), and mass-weighted terminal velocity (V_{tm}, m s^{-1}) were calculated (Figs. 8d–f). Using the polynomial least-square fit with weights of the rainwater content, mean curves (solid lines) for each parameter were derived in terms of liquid water content (g m^{-3}) and median volume diameter (mm) as follows:

$$R_e = W(0.0923D_0^{-3} - 0.309D_0^{-2} + 1.056D_0^{-1} - 0.0082) \times 10^{-3}, \tag{12}$$

$$R_a = W(-0.014D_0^3 + 0.211D_0^2 - 1.50D_0 + 7.04) \times 10^{-3}, \quad \text{and} \tag{13}$$

$$V_{tm} = 0.0916D_0^3 - 1.088D_0^2 + 4.754D_0 + 0.525. \tag{14}$$

As Fig. 8 shows, Eqs. (9)–(11) represent rain variables well for Z_{DR} ranging from 0.15 to 4 dB and Eqs. (12)–(14) are good empirical relations for R_e, R_a, and V_{tm} with D_0 less than 4 mm. To evaluate these empirical relations, we compare their results with observations. DSDs with a calculated Z_{DR} of 0.15–4 dB were used to validate Eqs. (8)–(11), and DSDs with a D_0 of 0.5–4 mm were used for Eqs. (12)–(14). Similar to Table 3, the bias and correlation coefficient values between empirical values and observed values were calculated and are listed in Table 4. One-to-one plots of these results (Fig. 9) reveals that Eqs. (13) and (14) for estimates of R_a (proportional to the 2.67th moment of the DSD) and V_{tm} have very small bias (<1%). Equations (9)–(11) for estimates of R, W, and D_0 have biases of less than 10%, and Eqs. (8) and (12) have biases of larger than 10%. This implies that empirical relations for low moments N_T (zero moment) and R_e (~1.6th moment) are not as good as relations for high moments. This is probably
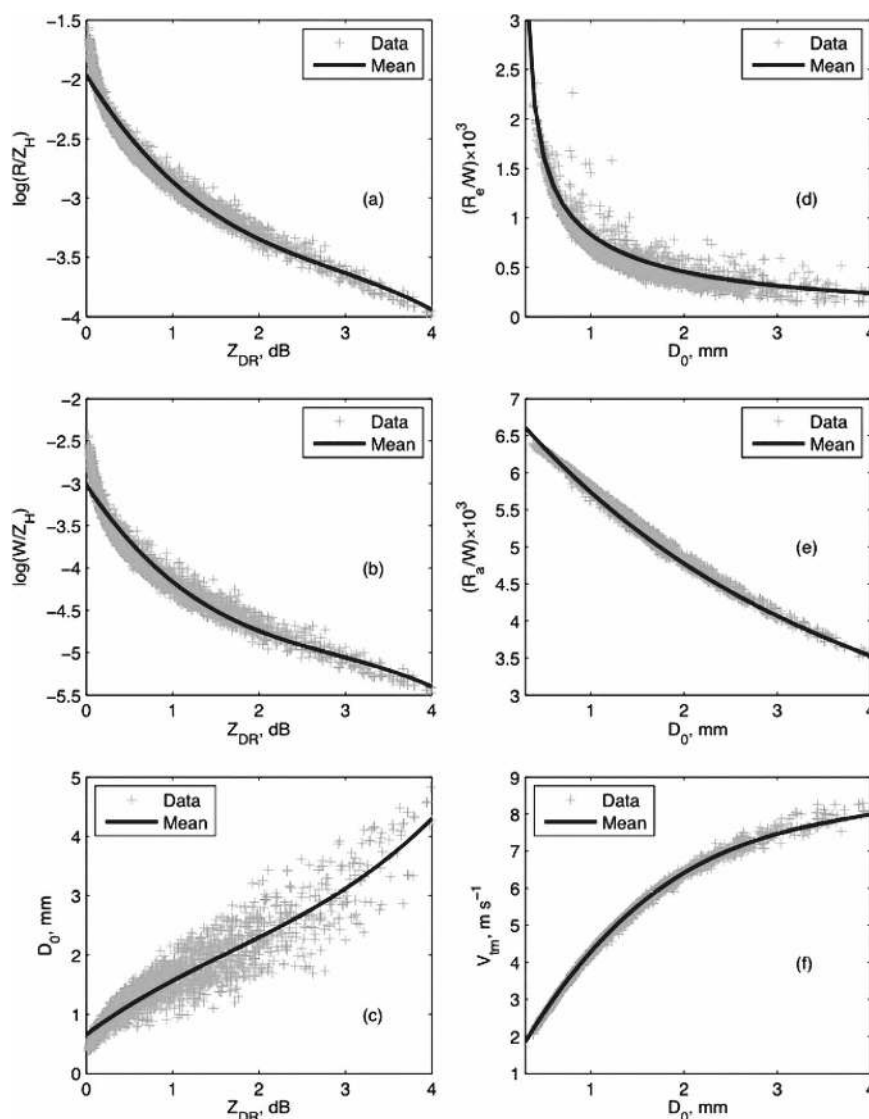
FIG. 8. Scatterplots of rain variables and radar variables calculated from 2DVD data. Solid lines are mean curves, which are fitted to data points by three-order polynomial fit. (a) Ratio of R to Z_H vs Z_{DR} [Eq. (9)], (b) ratio of W to Z_H vs Z_{DR} [Eq. (10)], (c) D_0 vs Z_{DR} [Eq. (11)], (d) ratio of R_e to W vs D_0 [Eq. (12)], (e) ratio of R_a to W vs D_0 [Eq. (13)], and (f) V_{tm} vs D_0 [Eq. (14)].

because the control variables (Z_H, Z_{DR}, W, and D_0) are mainly determined by middle-sized or large drops and they are not good at representing low moments. Middle moments (e.g., R_a and V_{tm}), on the other hand, are well represented. It is worth noting that the D_0–Z_{DR} plot (Fig. 8c) has large scatter. This likely results from the fact that the main contributor to D_0 is the large number of median-size drops, but Z_{DR} is mainly determined by a small number of large drops. This is also the reason why the D_0 estimated from Z_{DR}, when compared with the observed D_0, only has a correlation coefficient of approximately 0.8.

TABLE 4. Bias and correlation coefficient for rain variables using Eqs. (8)–(14) vs observations.

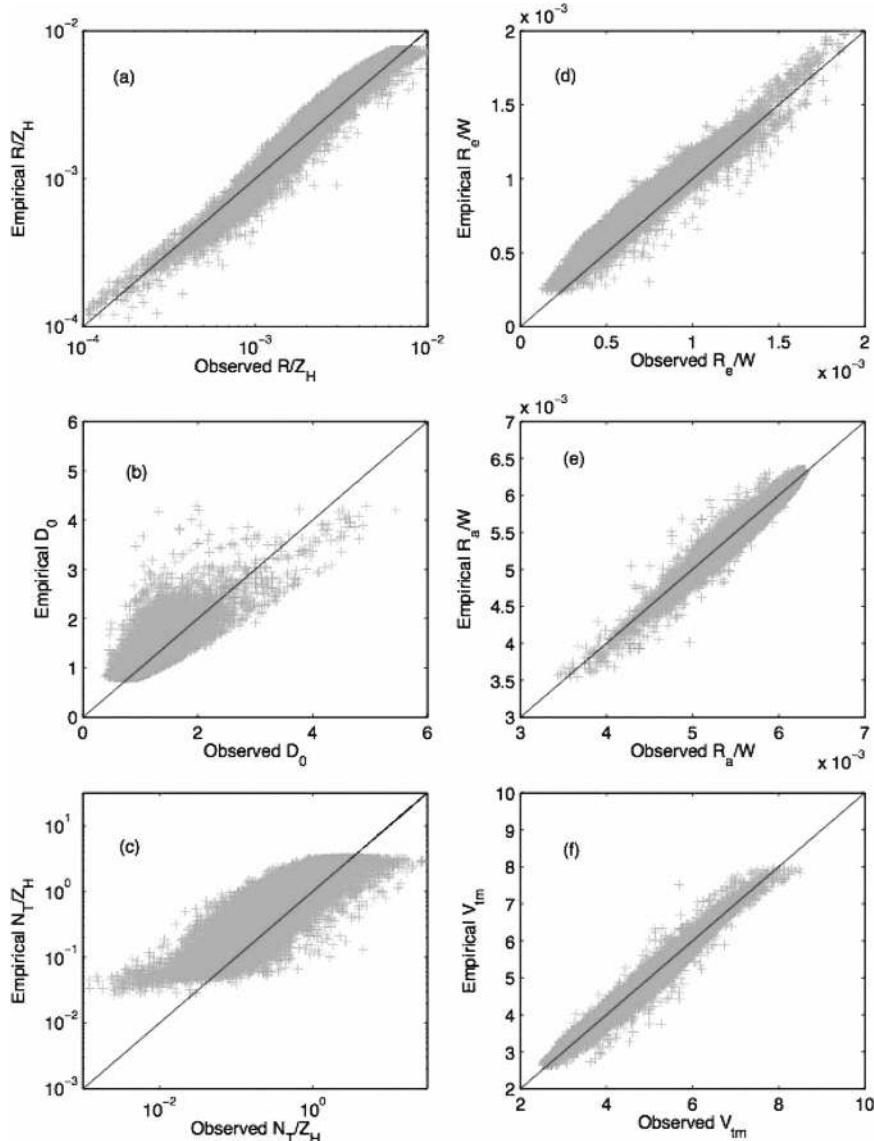|	N_T	R	W	D_0	R_e	R_a	V_{tm}
Bias (%)	20.24	9.09	9.63	7.18	13.80	−0.52	−0.026
Correlation coef	0.625	0.970	0.937	0.809	0.972	0.977	0.984

FIG. 9. One-to-one plots of empirical values vs observations. Crosses denote the data points, and solid lines correspond to the unit slope. Empirical relations are Eqs. (8)–(14). (a) Ratio of R to Z_H [Eq. (9)], (b) D_0 [Eq. (11)], (c) ratio of N_T to Z_H [Eq. (8)], (d) ratio of R_e to W [Eq. (12)], (e) ratio of R_a to W [Eq. (13)], and (f) V_{tm} [Eq. (14)].

3. Radar data analysis

a. Adjustment of disdrometer-based relation

The refined μ–Λ relation in section 2 enables the retrieval of the gamma DSD distribution parameters (N_0, μ, and Λ) from the measurements of radar reflectivity and differential reflectivity. A Z_H–Z_{DR} scatterplot calculated from disdrometer measurements is presented in Fig. 10. Solid and dashed lines denote polynomial fits for Oklahoma and Florida (Zhang et al. 2006), respectively. There is little difference between

these two curves for $Z_H < 30$ dBZ. The mean Z_H–Z_{DR} relation for Oklahoma is given by the equation

$$Z_{DR} = 10^{(-2.6857 \times 10^{-4} Z_H^2 + 0.04892 Z_H - 1.4287)}, \quad (15)$$

where both Z_H and Z_{DR} are expressed on a logarithmic scale. This Z_H–Z_{DR} relation (15) is consistent with the μ–Λ relation (7) in that both were derived from the same 2DVD measurements.

Previous studies (e.g., Schuur et al. 2001; Brandes et al. 2002, 2004a; Vivekanandan et al. 2004; Zhang et al.
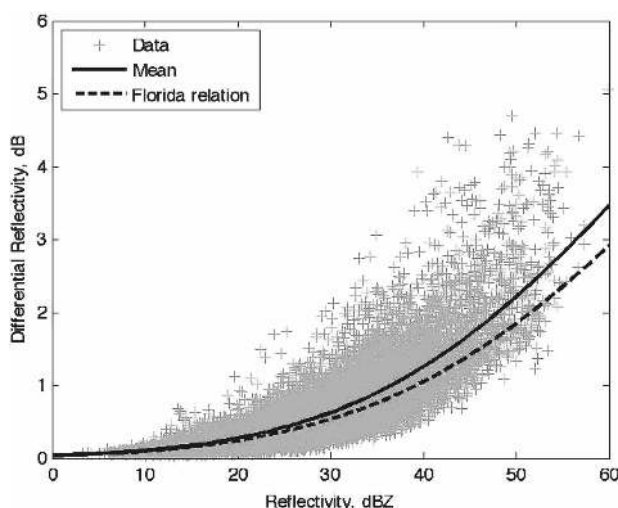
FIG. 10. Plot of Z_{DR} vs Z_H from 2DVD measurements in Oklahoma (using 14 200 1-min DSD data). Cross points denote 2DVD measurements. The solid line is the mean curve, which is fitted to all data points in logarithmic domain by two-order polynomial fit. The dashed line is the Florida relation (Zhang et al. 2001).

2006) have shown that disdrometer observations are generally consistent with radar observations and that DSD models derived from disdrometer observations generally work well when applied to radar retrieval. However, the sampling volume of a radar is much larger than that of a disdrometer. The KOUN, for example, has a sampling volume of $\sim$0.07 km^3 at a 30-km range. Consequently, its sampling volume can be 10^7 or more than that of 2DVDs. The difference between radar measurements and 2DVD measurements might be large, especially for inhomogeneous rains (e.g., at the leading edge of convection). The radar retrieval may not work well if Z_H and Z_{DR} measurements depart significantly from the disdrometer-based mean relation. Figure 11a shows a plan position indicator (PPI) image of radar reflectivity measured by KOUN on 13 May 2005. A solid square isolates a strong convective cell at the leading edge of the squall line. The dashed region includes portions of the leading and trailing convective line. The scatterplots of Z_H and Z_{DR} within these two regions are plotted in Fig. 11b. The disdrometer-based mean Z_H–Z_{DR} relation in Eq. (15) is plotted for reference. Most Z_H–Z_{DR} pairs from the rectangular box cluster well around the line described by Eq. (15) except for the measurements corresponding to the isolated convective cell, where relatively high Z_{DR} are associated with relatively low Z_H. According to the hydrometeor classification algorithm described by Ryzhkov et al. (2005), these points are identified as rain dominated by "big drops" (BDs). In the BD region, the
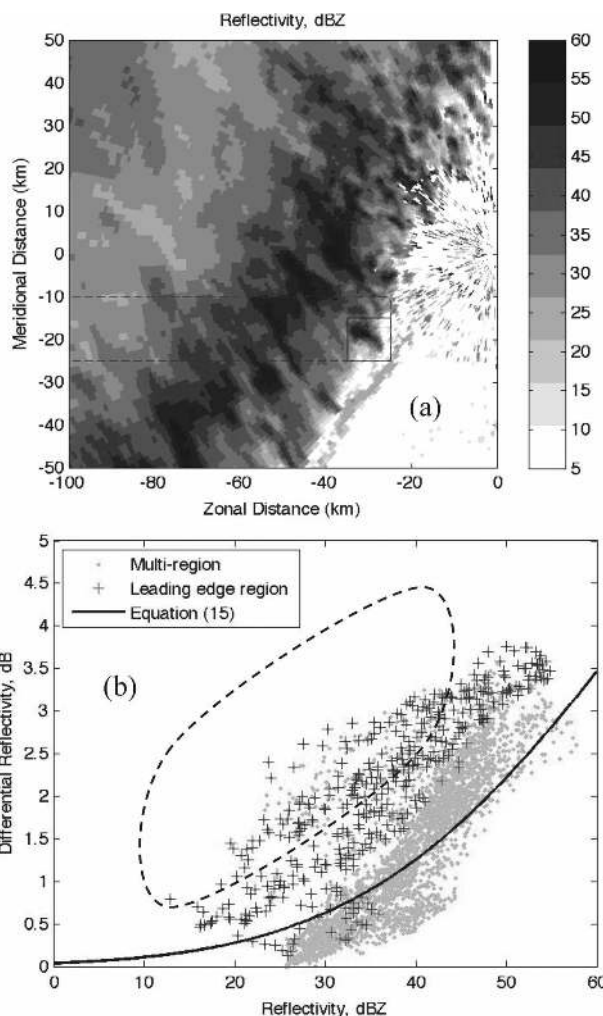

FIG. 11. (a) PPI of KOUN radar-measured reflectivity (0659:55 UTC 13 May 2005). A solid square isolates a strong convective storm at the leading edge of this rain event. The dashed rectangular region is a multiple precipitation-type region that includes portions of the convective leading edge, thunderstorm core, and trailing stratiform precipitation. (b) Scatterplot of Z_{DR} vs Z_H. Dots denote measurements within the multiple precipitation-type region [dashed-line region of (a)]. Asterisks denote measurements within leading edge region [solid-line square of (a)]. The solid line is the mean curve of disdrometer observations (solid line of Fig. 10). The region within the dashed line includes BD cases.

DSD tends to be narrower and the total concentration of drops tends to be much lower than in stratiform rain with the same intensity. Retrievals based on Eq. (7) may result in errors in the BD regions. For example, such a retrieval would result in broadly estimated DSDs and an unreasonably large total number concentration. To solve this problem, the disdrometer-based relation is adjusted to

$$\mu = \mu'(\Lambda) + C\Delta Z_{DR}, \quad (16)$$

where the $\mu'(\Lambda)$ is the disdrometer-based relation in Eq. (7) derived in the previous section, ΔZ_{DR} is the difference between the radar-measured Z_{DR} and the Z_{DR} estimated from the measured Z_H according to Eq. (15), and C is an adjustment parameter. It is reasonable to consider that the adjustment term $C\Delta Z_{DR}$ is related to Z_H and Z_{DR} because Z_H and Z_{DR} give useful information about rain type, intensity, and the DSD. Intuitively, the adjustment parameter C should be positive and dependent on Z_H and Z_{DR}. For a given ΔZ_{DR}, C should increase when Z_{DR} increases or Z_H decreases. It is hard, however, to determine a good adjustment term that fully represents the variability of rain physics. In this study, we focus on the adjustment of BD regions, where the ΔZ_{DR} has a maximum dynamic range of 3. We expect the adjusted μ to fall into the normal dynamic range of 6; accordingly, the value of C was chosen to be 2 for this study. No adjustment is made if $\Delta Z_{DR} < 0.5$ dB. The adjustable $\mu-\Lambda$ relation could improve the retrieval of N_T and D_0 at the leading edges of convective squall lines, which are often characterized by BD regions. On the other hand, the effect of the adjustment is minor outside of the BD regions.

b. Radar retrieval

The radar retrieval was applied to the rain event illustrated in Fig. 11a. The retrieval was performed over the whole storm area (including the BD region) using radar-measured Z_H and Z_{DR} and a refined $\mu-\Lambda$ relation with adjustment [i.e. Eq. (16)]. The retrieval without adjustment was also performed as a comparison. The retrieval procedure is similar to that described in previous studies (e.g., Zhang et al. 2001; Brandes et al. 2004a) except for the numerical method used to solve the nonlinear equations and the procedure to estimate the maximum diameter. The regression method used here is the two-dimensional Newton–Raphson method (Press et al. 2001, 355–361). The maximum diameter in previous studies was estimated from an empirical relation fitted to disdrometer observations (e.g., Brandes et al. 2004a), which remains as an issue in radar retrieval. When the $\mu-\Lambda$ relation is used with the adjustment, the impact of the maximum diameter is minimal. Therefore, we set the maximum diameter to a constant of 8 mm, which works for most rain events ($Z_H < 60$ dBZ).

The PPI fields of radar measurements and retrieval results are shown in Fig. 12. The fields of Z_H and Z_{DR} and the results of hydrometer classification [no rain echo (NR), light and moderate rain (R), heavy rain (HR), rain–hail mixture (RH), and big drops (BD); Ryzhkov et al. (2005)] are shown in column A. Measurements of Z_H and Z_{DR} classified as NR or RH were filtered out before the rain retrievals were performed.

Column B contains retrieval results based on the $\mu-\Lambda$ relation without adjustment [Eq. (7)], and Column C represents retrieval results based on the $\mu-\Lambda$ relation with adjustment [Eq. (16)]. These two approaches give similar and reasonable retrievals for most of the duration of the storm. It is noted that retrieved rain rates through two approaches show little difference. In general, the $\mu-\Lambda$ adjustment mainly reduces the number concentration of small drops while causing less change for median and large drops. Consequently, lower moments are affected more than higher moments. The rain rate, which is mainly determined by drops of median sizes, is approximated by the 3.67th moment. In addition, the two-parameter retrieval already yields accurate rain estimation; hence, the retrieved rain rate is less affected by the adjustment. In BD regions with low Z_H, however, retrievals without $\mu-\Lambda$ adjustment produce much higher N_T and smaller D_0. According to retrievals without adjustment, a large number of small drops exist in the area where a small number of big drops should be. Thus, retrievals with adjustments give more reasonable results for developing convective cells.

The refined $\mu-\Lambda$ relation in Eq. (7) has already been verified by disdrometer data in section 2 (Fig. 7 and Table 3). In the next section, comparisons between radar retrievals and disdrometer observations are made to demonstrate the utility of the radar data. The rain event analyzed was a precipitation system that passed over central Oklahoma on 2 May 2005, when the NCAR 2DVD was deployed 28 km south of KOUN. Figure 13 shows the time series of Z_H and Z_{DR} from 1100 to 1330 UTC. The asterisks denote radar measurements. To reduce error, radar measurements have been averaged over five range gates. To eliminate a systematic bias between radar and disdrometer, the radar-measured Z_{DR} was adjusted by subtracting 0.3 dB. Possible contamination from a low melting layer and ground targets was mitigated by removing data points with a cross correlation coefficient of less than 0.9. The solid lines denote Z_H and Z_{DR} calculated from disdrometer observations. Figure 13 shows that disdrometer calculations match the radar measurements quite well. The discrepancy between radar measurements and disdrometer calculations during some short periods (e.g., at 1140 and 1320 UTC) is attributed to the inhomogeneity in the rain's spatial distribution.

Using the C-G DSD model, rain parameters were retrieved from dual-polarization radar measurements. Figure 14 shows the comparison of R, D_0, and N_T between radar retrievals and disdrometer calculations. The asterisks denote radar retrievals and the solid lines denote disdrometer calculations from observed DSDs. Referring to Fig. 13, if the radar-measured Z_H and Z_{DR}
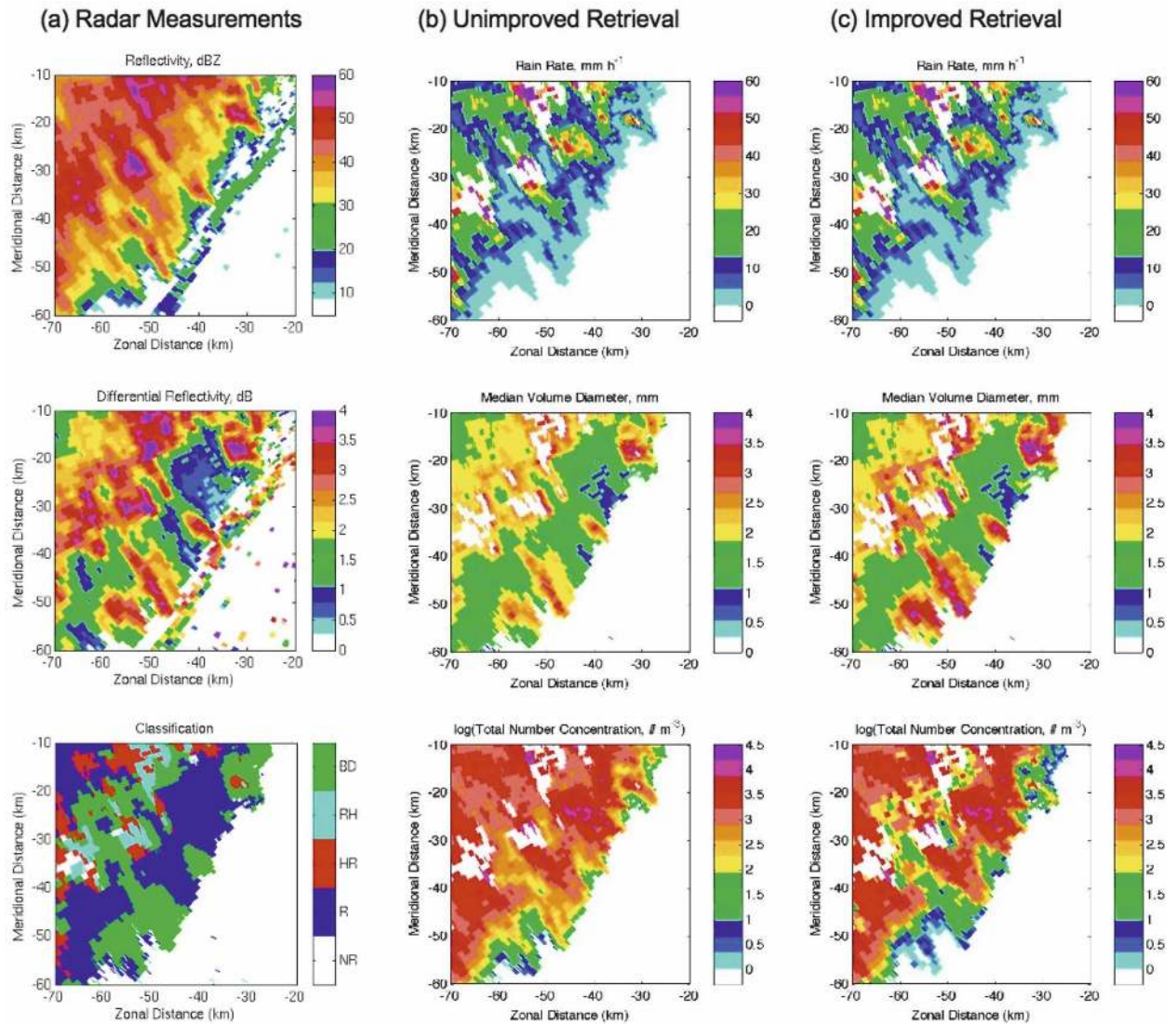
FIG. 12. Comparison of radar retrievals based on adjusted and unadjusted μ–Λ relation. Column A shows radar-measured reflectivity and differential reflectivity (0659:55 UTC 13 May 2005), and classifications of rain [no rain echo (NR), light and moderate rain (R), heavy rain (HR), rain–hail mixture (RH), and big drops (BD)]. Reflectivity and differential reflectivity measurements classified as NR and RH were filtered out before the rain retrievals were performed. Column B (C) shows radar retrieval results of rain rate, median volume diameter, and total number concentration based on the refined μ–Λ relation without (with) adjustment; Eqs. (7) and (16), respectively.

agree with the disdrometer measurements, the retrieved rain variables in Fig. 14 match the disdrometer measurements. Compared to retrieval results in a previous study (Cao et al. 2006, their Fig. 7), the retrieval of the median volume diameter has improved, especially for periods of light rain. The values of N_T for light rain are also close to disdrometer observations. Considering the sampling volume difference between radar and disdrometer, the refined disdrometer-based μ–Λ relation (7) is believed to give a satisfactory retrieval from polarimetric radar measurements. In addition, the

adjustment of the μ–Λ relation [Eq. (15)] gives a reasonable retrieval for rains of BD cases.

4. Conclusions and discussion

In this paper, 2D-video disdrometer and polarimetric radar data are used to characterize rain microphysics in Oklahoma. The 2DVD measurement errors are investigated and quantified through a side-by-side comparison with two instruments and then minimized using a sorting and averaging method (SATP). Based on
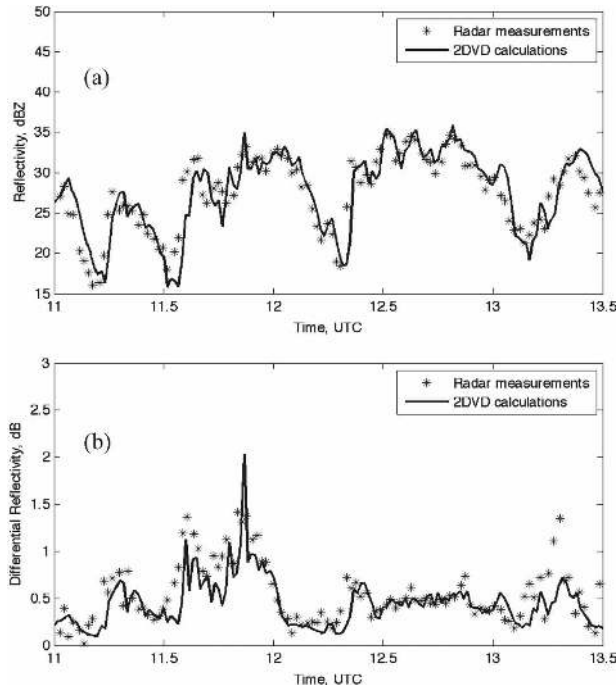
FIG. 13. Comparison of radar measurements and disdrometer calculations for (a) reflectivity and (b) differential reflectivity. Asterisks denote radar measurements on 2 May 2005. Solid lines denote that reflectivity and differential reflectivity are calculated from observed DSDs by 2DVD.
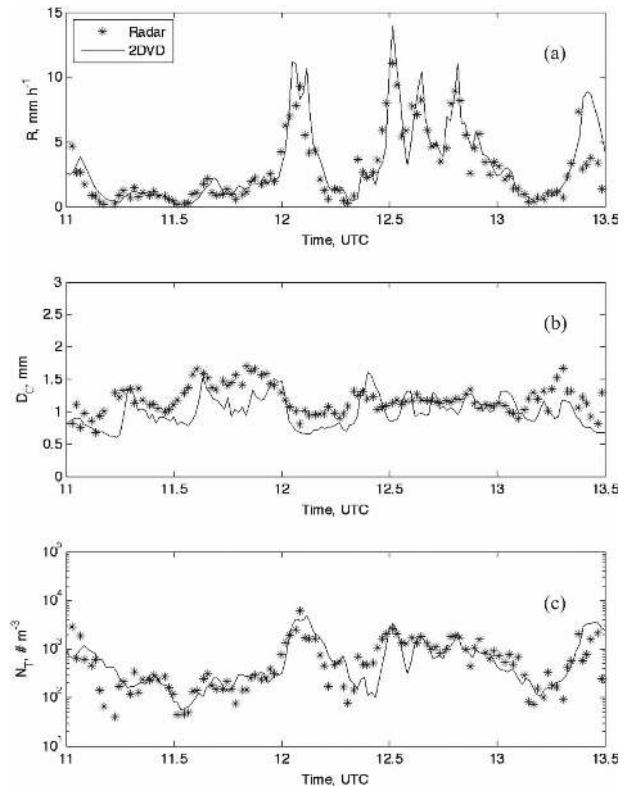

FIG. 14. Comparisons of (a) rain rate, (b) median volume diameter, and (c) total number concentration from radar retrievals (asterisks) and disdrometer observations (solid lines) for 2 May 2005.

SATP, the μ–Λ relation of the C-G DSD model is refined and verified by disdrometer data. An adjustment of the μ–Λ relation is introduced to solve the problem of radar retrieval for BD cases. The refined μ–Λ relation is then applied to polarimetric radar retrieval and evaluated by comparison with the disdrometer observations.

In 2DVD measurements, sampling errors of large drops have been found to be substantial and dominated by statistical errors and sampling errors of very small drops are mainly attributed to system limitations. Middle DSD moments (e.g., the third moment), on the other hand, have comparatively smaller sampling errors than the outer moments (e.g., the zero moment or the sixth moment). Although two adjacent moments have highly correlated sampling errors, there is little correlation if the order difference of the two moments is larger than 3. The sampling error may also affect moment-based empirical relations. For example, TMF uses the second, fourth and sixth moments to fit DSD shape and slope. The combination of these three moments, however, may not be optimal. Carefully choosing different moments may help to reduce the effect of sampling errors, which is worth further investigation.

The SATP method was introduced to reduce statis-

tical errors of 2DVD observations and improve the C-G DSD model. Compared to other filtering methods applied to disdrometer observations (Lee and Zawadzki 2005; Sauvageot and Lacaux 1995), SATP has the following advantages: (i) It identifies (or isolates) similar DSDs; (ii) statistical errors of observed DSDs can be reduced while physical variations are preserved; (iii) it is applicable to more than one rain event; and (iv) the performance of SATP improves as the size of the dataset increases. There are also limitations to the application of SATP: (i) Two parameters are not accurate enough to characterize some extreme cases (e.g., nongamma distributions); (ii) different combinations of two parameters may affect the retrieved DSD; (iii) averaging the DSDs may reduce the physical variation if the grid pixels are not small enough; and (iv) the dataset is small for extremely heavy rain, which limits the utility of SATP. In spite of these limitations, SATP is a promising method for processing disdrometer data. Possibly SATP can be improved if more parameters (e.g., three parameters) are used to characterize DSDs. However, the size of the current dataset is not sufficient for sorting based on more than two parameters.

In this study, the C-G DSD model was further proved to be valid for DSD retrieval by the analysis of disdrometer observations collected in Oklahoma. The refined μ–Λ relation in Eq. (7) gives better representation of rain characteristics. The relation can be used within the range of 0 to 20 for Λ. It is suggested that Eqs. (8)–(11) be used for Z_{DR} ranging from 0.15 to 4 dB and Eqs. (12)–(14) for D_0 less than 4 mm. The relations should be useful for model parameterization and data assimilation.

The principal limitation of the C-G DSD model is that it only has 2 degrees of freedom with which to characterize DSDs. Nevertheless, the model should yield satisfactory retrievals of rain variables (R and D_0) and microphysical processes (R_e and R_a) for most rain events. However, in cases with bimodal DSDs, long tails, and BD, the retrievals may not match the observations and the retrieved rain variables will have large deviations. For BD cases, retrievals based on Eq. (7) will overestimate N_T and underestimate D_0. Adjustment of the μ–Λ relation according to Eq. (16) is proposed to give better retrievals of N_T and D_0. Although the adjustment is coarse, it is believed to improve the retrieval for the leading edge of convection. The C-G model might be further improved by combining additional information such as temporal and spatial correlations, more observations, and prior statistical information.

REFERENCES

Brandes, E. A., G. Zhang, and J. Vivekanandan, 2002: Experiments in rainfall estimation with a polarimetric radar in a subtropical environment. *J. Appl. Meteor.,* **41,** 674–685.
——, ——, and ——, 2004a: Drop size distribution retrieval with polarimetric radar: Model and application. *J. Appl. Meteor.,* **43,** 461–475.
——, ——, and ——, 2004b: Comparison of polarimetric radar drop size distribution retrieval algorithms. *J. Atmos. Oceanic Technol.,* **21,** 584–598.
——, T. J. Schuur, A. Ryzhkov, G. Zhang, and K. Ikeda, 2005: Rain microphysics retrieval with a polarimetric WSR-88D. Preprints, *32nd Conf. on Radar Meteorology,* Albuquerque, NM, Amer. Meteor. Soc., 9R.2. [Available online at http://ams.confex.com/ams/pdfpapers/97017.pdf.]

Bringi, V. N., G. Huang, V. Chandrasekar, and E. Gorgucci, 2002: A methodology for estimating the parameters of a gamma raindrop size distribution model from polarimetric radar data: Application to a squall-line event from the TRMM/Brazil campaign. *J. Atmos. Oceanic Technol.,* **19,** 633–645.
——, V. Chandrasekar, J. Hubbert, E. Gorgucci, W. L. Randeu, and M. Schoenhuber, 2003: Raindrop size distribution in different climatic regimes from disdrometer and dual-polarized radar analysis. *J. Atmos. Sci.,* **60,** 354–365.

Cao, Q., G. Zhang, T. Schuur, A. Ryzhkov, E. Brandes, and K. Ikeda, 2006: Characterization of rain microphysics based on disdrometer and polarimetric radar observations. *Proc. IGARSS 2006,* Denver, CO, IEEE, 02_11A05.

Chandrasekar, V., and V. N. Bringi, 1987: Simulation of radar reflectivity and surface measurements of rainfall. *J. Atmos. Oceanic Technol.,* **4,** 464–478.

Gertzman, H. S., and D. Atlas, 1977: Sampling errors in the measurements of rain and hail parameters. *J. Geophys. Res.,* **82,** 4955–4966.

Gorgucci, G., V. Chandrasekar, V. N. Bringi, and G. Scarchilli, 2002: Estimation of raindrop size distribution parameters from polarimetric radar measurements. *J. Atmos. Sci.,* **59,** 2373–2384.

Haddad, Z. S., D. A. Short, S. L. Durden, E. Im, S. H. Hensley, M. B. Grable, and R. A. Black, 1997: A new parameterization of the rain drop size distribution. *IEEE Trans. Geosci. Remote Sens.,* **35** (3), 532–539.
——, J. P. Meagher, S. L. Durden, E. A. Smith, and E. Im, 2006: Drop size ambiguities in the retrieval of precipitation profiles from dual-frequency radar measurements. *J. Atmos. Sci.,* **63,** 204–217.

Jameson, A. R., and A. B. Kostinski, 1998: Fluctuation properties of precipitation. Part II: Reconsideration of the meaning and measurement of raindrop size distributions. *J. Atmos. Sci.,* **55,** 283–294.

Joss, J., and E. G. Gori, 1978: Shapes of raindrop size distributions. *J. Appl. Meteor.,* **17,** 1054–1061.

Kozu, T., and K. Nakamura, 1991: Rain parameter estimation from dual-radar measurements combining reflectivity profile and path-integrated attenuation. *J. Atmos. Oceanic Technol.,* **8,** 259–270.

Lee, G., and I. Zawadzki, 2005: Variability of drop size distributions: Time-scale dependence of the variability and its effects on rain estimation. *J. Appl. Meteor.,* **44,** 241–255.

Press, W. H., S. A. Teukolsky, W. T. Vetterling, and B. P. Flannery, 2001: *Numerical Recipes in FORTRAN 77.* 2nd ed. Cambridge University Press, 963 pp.

Ryzhkov, V. A., T. J. Schuur, D. W. Burgess, P. L. Heinselman, S. E. Giangrande, and D. S. Zrnić, 2005: The Joint Polarization Experiment: Polarimetric rainfall measurements and hydrometeor classification. *Bull. Amer. Meteor. Soc.,* **86,** 809–824.

Sauvageot, H., and J. Lacaux, 1995: The shape of averaged drop size distributions. *J. Atmos. Sci.,* **52,** 1070–1083.

Schuur, T. J., A. V. Ryzhkov, D. S. Zrnić, and M. Schönhuber, 2001: Drop size distributions measured by a 2D video disdrometer: Comparison with dual-polarization radar data. *J. Appl. Meteor.,* **40,** 1019–1034.

Tokay, A., A. Kruger, and W. F. Krajewski, 2001: Comparison of

drop size distribution measurements by impact and optical disdrometers. *J. Appl. Meteor.,* **40,** 2083–2097.

Ulbrich, C. W., 1983: Natural variations in the analytical form of the raindrop size distribution. *J. Climate Appl. Meteor.,* **22,** 1764–1775.

——, and D. Atlas, 1998: Rainfall microphysics and radar properties: Analysis methods for drop size spectra. *J. Appl. Meteor.,* **37,** 912–923.

Vivekanandan, J., G. Zhang, and E. Brandes, 2004: Polarimetric radar estimators based on a constrained gamma drop size distribution model. *J. Appl. Meteor.,* **43,** 217–230.

Wong, R. K. W., and N. Chidambaram, 1985: Gamma size distri-

bution and stochastic sampling errors. *J. Appl. Meteor.,* **24,** 568–579.

Zhang, G., J. Vivekanandan, and E. Brandes, 2001: A method for estimating rain rate and drop size distribution from polarimetric radar measurements. *IEEE Trans. Geosci. Remote Sens.,* **39** (4), 830–840.

——, ——, ——, R. Meneghini, and T. Kozu, 2003: The shape–slope relation in gamma raindrop size distributions: Statistical error or useful information? *J. Atmos. Oceanic Technol.,* **20,** 1106–1119.

——, J. Sun, and E. Brandes, 2006: Improving parameterization of rain microphysics with disdrometer and radar observations. *J. Atmos. Sci.,* **63,** 1273–1290.